Journal of Nuclear Materials 389 (2009) 351–358

Contents lists available at ScienceDirect

Journal of Nuclear Materials

journal homepage: www.elsevier.com/locate/jnucmat

Characterization of ThO_2–UO_2 pellets made by co-precipitation process

T.R.G. Kutty [a,*], K.B. Khan [a], P.V. Achuthan [b], P.S. Dhami [b], A. Dakshinamoorthy [b], P.S. Somayajulu [c], J.P. Panakkal [c], Arun Kumar [a], H.S. Kamath [d]

[a] Radiometallurgy Division, Bhabha Atomic Research Centre, Trombay, Mumbai 400 085, India
[b] Fuel Reprocessing Division, Bhabha Atomic Research Centre, Trombay, Mumbai 400 085, India
[c] Advanced Fuel Fabrication Facility, Tarapur, Bhabha Atomic Research Centre, Trombay, Mumbai 400 085, India
[d] Nuclear Fuels Group, Bhabha Atomic Research Centre, Trombay, Mumbai 400 085, India

ARTICLE INFO

Article history:
Received 15 January 2008
Accepted 3 December 2008

PACS:
81.20.Ev
61.72.–y
62.20.Fe
81.70.P

ABSTRACT

The co-precipitation technique renders an excellent route to obtain a homogeneous mixture of ThO_2 and UO_2 powders. In this process, after the nitrate solutions of Th and U are mixed in the intended ratio, oxalic acid is added for co-precipitation. The precipitate is then dried and calcined to get a solid solution of ThO_2 and UO_2. In this study, ThO_2–30%UO_2 and ThO_2–50%UO_2 (% in weight) powders were characterized in terms of particle size, particle shape, surface area, phase content, O/M ratio etc. The pellets obtained by sintering these powders were characterized with the help of optical microscopy, scanning electron microscopy (SEM) and electron probe microanalysis (EPMA). The XRD data for ThO_2–30%UO_2 and ThO_2–50%UO_2 pellets showed the presence of a small amount of U_3O_8 phase besides fluorite phase. The grain size of ThO_2–30%UO_2 and ThO_2–50%UO_2 was found to be 5.7 and 4.5 μm, respectively.

1. Introduction

In manufacturing the mixed oxide fuels like $(Pu,U)O_2$ and $(Th,^{233}U)O_2$, the homogeneous distribution of the constituent metals is an important point to be studied, since it relates to the safety and reliability of the fuel [1–5]. The requirement for high homogeneity of the distribution of the actinides in the fuel is also essential for most of new generation (Gen IV) reactors. Traditionally, (Th–U)O_2 pellets are made by powder metallurgy technique consisting of blending of ThO_2 and UO_2 powders followed by milling, compaction and sintering in reducing atmosphere at around 1700 °C [6,7]. The key step in the production of the above mixed oxide fuels is the preparation of homogeneous oxide mixtures [8]. The presence of fissile rich regions in a pellet affects the fuel performance since they act as hot spots generating high temperatures and releasing more fission gases [9,10]. For PuO_2–UO_2 fuel of thermal reactors, therefore, the maximum size of Pu rich agglomerate is specified under the Pu dispersion criterions [11]. Generally, the specifications define the maximum Pu rich agglomerate size corresponding to pure PuO_2 particle of 400 μm in diameter. The Pu dispersion criterion prescribes that no more than 5% of the nominal PuO_2 content within a pellet shall be present in PuO_2 rich particles with equivalent diameters of 100 μm or greater [11]. The presence of fissile rich region also causes a problem during the reprocessing operations since these pellets will not dissolve completely in nitric acid without the addition of hydrofluoric acid. Hence, it is essential to avoid the formation of such fissile rich regions by adopting the proper manufacturing procedures. The blending and sintering technologies play the most important role for having the pellets with high micohomogeneities [12]. The sophistication in blending readily improves homogeneity. The manufacturers have made great efforts in optimizing blending technology by using high energy mills, attritors etc. Another way to improve the homogeneity is the progressive dilution of PuO_2 to UO_2 or $^{233}UO_2$ to ThO_2 instead of the process of direct mixing [11]. But all the above mentioned procedures do not guarantee the absence the fissile rich zones in the pellets.

Fabrication of Pu-bearing mixed oxide fuels (MOX) for light water reactors (LWRs) has now been mastered industrially by many countries [13]. MIMAS is the common MOX fuel manufacturing process used at Dessel and Cadarache plants. BNFL followed Short Binderless Route (SBR) which uses a high energy attritor mill to blend uranium oxide and plutonium oxide feed powders, and a spheroidiser to condition the powder before it is fed to the press [13,14]. However, for the fabrication fuels containing highly radioactive materials, such as reactor grade plutonium, ^{233}U, americium, curium etc., the problem of dust generation and consequent radiation exposure to personnel becomes more serious causing to limit the application of the powder processes. Further, the fine powders are not free flowing, which poses another problem in remote and automated fabrication. The hazard, therefore, to be considered for workers are dust particulates becoming airborne and entering the human body. Therefore, alternative fabrication routes are to

* Corresponding author. Tel.: +91 22 2559 5361; fax: +91 22 2550 5151.
E-mail address: tkutty@barc.gov.in (T.R.G. Kutty).

0022-3115/$ - see front matter © 2009 Elsevier B.V. All rights reserved.
doi:10.1016/j.jnucmat.2008.12.334

be envisaged. The wet synthesis methods present a reduced hazard since the major part of the process is done in liquid form prior to powder handling. In addition, the morphology of the particles made by the wet route is largely spherical; which smoothly move and are easily filled in dies for pelletization.

Among the various techniques, the co-precipitation method gives an excellent route to make a very homogeneous mixture. It is reported that PuO_2–UO_2 green pellet fabricated from co-precipitated feeds form a solid solution at about 1000 °C in hydrogen and are completely soluble in nitric acid up to 40% Pu/HM (heavy metal) [11]. On the other hand, for the pellets prepared from mechanically mixed powders, the solid solution formation is completed only at about 1700 °C, but have recurrent problems with respect to the specifications for solubility in nitric acid. The co-precipitation process had been given a low priority by fuel manufacturers since it involves handling of the liquid waste. However, if the co-precipitation process is incorporated in the reprocessing plant, then this method would become really advantageous [15]. The advantages of the wet process include [11,15–18]:

1. Very low generation of radiotoxic dust.
2. Easy availability of cheap reactants.
3. Reduction of the accessibility to pure plutonium or other fissile actinides, and reduction of risks of proliferation.
4. This method is easily amenable for glove box operation.

In India the amount of thorium reserves is about five times larger than that of uranium. These very large thorium resources could be utilized for nuclear energy generation apart from the efficiency increase in uranium resource utilization. ^{232}Th is a better fertile material than ^{238}U in thermal reactors. The neutron yield of ^{233}U in the thermal and epithermal regions is higher than those of ^{235}U and ^{239}Pu. The currently known Indian thorium reserves amount to 358,000 GWe-yr of electrical energy, which can easily satisfy the energy requirements during the next century and beyond [19]. Accordingly, while formulating the national programme, thorium has been envisaged as the fuel for the third and the largest phase of Indian nuclear power programme. India is currently engaged in the design of a thorium fuelled Advanced Heavy Water Reactor (AHWR) for generation of power. The reactor physics design of AHWR is tuned to generate about 75% power in thorium, and is to maintain negative void coefficient of reactivity under all operating conditions [20,21]. The aim of this work is to develop the co-precipitation technique to fabricate ThO_2–30%UO_2 and ThO_2–50%UO_2 fuel pellets, where % is given as wt%. So far, detailed studies have not been reported on above mentioned compositions by co-precipitation route. Characterization was made for the microstructures by using XRD, TG, DTA, SEM and EPMA techniques.

2. Previous work

A number of reports are available on the production of uranium–plutonium mixed oxide by co-precipitation method but information on thorium–uranium mixed oxide using the above method is scanty [1,22–27]. In AECL, studies were made for the co-precipitation process using ammonia [22]. To the nitrate solution of U(VI) and Th(IV), ammonia solution was added to form ammonium diuranate and thorium hydroxide co-precipitate. The precipitate is calcined to form blended ThO_2 and UO_2 powder, which is subsequently pressed into fuel pellets. Radford et al. [1] prepared ThO_2–6 wt%UO_2 powders by the co-precipitation from mixed nitrate solution using NH_4OH. They changed the calcination temperature and studied the physical properties of the obtained pellets. Atlas et al.[23] prepared ThO_2–20 wt%UO_2 pellets via co-precipitation of mixed oxalate from nitrate solutions by adding excess oxalic acid and studied various parameters which may affect the powder properties. White et al. [28] investigated precipitation temperature, agitation and digestion time for the preparation of ThO_2–25% UO_2. Argo [29] prepared ThO_2–20%UO_2, ThO_2–35%UO_2 and ThO_2–50%UO_2 pellets (% in weight) by the co-precipitation method. Here, U(VI) nitrate solution was first reduced to U(IV) by adding a sixfold excess sodium formaldehyde sulfoxylate at room temperature. To form the co-precipitate, oxalic acid of sixfold excess of the stoichiometric amount, dissolved in distilled water was added to the mixed nitrate solution of Th(IV) and U(IV). The precipitate was separated by vacuum filtration and dried in air at room temperature.

3. Experimental

The procedure of this work for the fabrication of ThO_2–30%UO_2 and ThO_2–50%UO_2 powders by co-precipitation route consists of the following steps:

(a) Preparation uranyl and thorium nitrate solution.
(b) Reduction of U ions from (VI) to (IV) valency state.
(c) Mixing of the solutions to the intended U to Th ratio.
(d) Co-precipitation using oxalic acid.
(e) Calcination.

3.1. Fabrication of ThO_2–UO_2 powders

The starting solutions used in this study are uranyl nitrate and thorium nitrate solutions. The concentration of uranyl nitrate solution was 200 g/l (in 1 M HNO_3) while that of thorium nitrate was 300 g/l in water. The oxidation states of thorium and uranium were 4+ and 6+, respectively. For having fine co-precipitates, the precipitation velocity and the solubility product of the oxalates of each metal need to be close. This condition is satisfied for Th(IV) and U(IV) oxalates. But the solubility product is much differed for U(VI) oxalate. Therefore, uranium was reduced to U(IV) in the initial stage to get a homogeneous product [30,31]. The reduction of uranyl nitrate solution was carried out by hydrazine with the help of platinum oxide as a catalyst. The product obtained after reduction contained more than 96% U (IV) in ~0.1 M N_2H_4 and 0.4 M HNO_3. Then, U(IV) and Th(IV) nitrate solutions were mixed into the specified U:Th ratio.

The precipitation experiment was carried out in 2 l batches with 10% oxalic acid (0.79 M) solution. The oxalic acid of 0.1 M excess amount was used. The precipitation reaction can be represented by the following equation:

$$(1-y)\mathrm{Th}(\mathrm{NO_3})_4 + y\mathrm{U}(\mathrm{NO_3})_4 + 2\mathrm{H_2C_2O_4} \rightarrow [(1-y)\mathrm{Th}(\mathrm{C_2O_4})_2 + y\mathrm{U}(\mathrm{C_2O_4})_2] \cdot n\mathrm{H_2O} + 4\mathrm{HNO_3} \quad (1)$$

where y is the mole fraction of uranium.

The $(Th,U)(C_2O_4)_2$ nH_2O precipitate from the above equation was then allowed to settle for 2 h and vacuum filtered through a SS frit. The precipitate was washed with 500 ml of distilled water. It was then heated to 200 °C in 1 h and then held at that temperature for 1 h, which results in decomposition of the oxalates to carbonates by the following reactions [30]:

$$[(1-y)\mathrm{Th}(\mathrm{C_2O_4})_2 + y\mathrm{U}(\mathrm{C_2O_4})_2]n\mathrm{H_2O} \rightarrow [(1-y)\mathrm{Th}(\mathrm{C_2O_4})_2 + y\mathrm{U}(\mathrm{C2O_4})_2] + n\mathrm{H_2}O \quad (2)$$

$$[(1-y)\mathrm{Th}(\mathrm{C_2O_4})_2 + y\mathrm{U}(\mathrm{C_2O_4})_2] \rightarrow [(1-y)\mathrm{Th}(\mathrm{CO_3})_2 + y\mathrm{U}(\mathrm{CO_3})_2] + 2\mathrm{CO} \quad (3)$$

The resulted mixture was heated from 200 °C to 700 °C with a heating rate of 4 K/min and soaked at 700 °C for 3 h. This results in formation of mixed oxide phases by the following reaction:

$$[(1-y)\mathrm{Th}(\mathrm{CO_3})_2 + y\mathrm{U}(\mathrm{CO_3})_2] \rightarrow [(1-y)\mathrm{ThO_2} + y\mathrm{UO_{2+x}}] + xy\mathrm{CO} + (2-xy)\mathrm{CO_2} \quad (4)$$

About 2 kg each of the mixed oxides of composition ThO_2–30%UO_2 and ThO_2–50%UO_2 (% in weight) were prepared. Thorium and uranium lost in the above process were less than 1.5 and 1.2 mg/l, respectively. The chemically analyzed values of thorium and uranium are given in Table 1. Table 2 gives the typical impurity contents of co-precipitated powders. The major advantage of the above co-precipitation method is the decontamination from Fe which is normally encountered in the final product solution received from the reprocessing plant [30]. In the ADU route, a separate step was necessary to remove Fe by carbonate precipitation prior to the uranium precipitation.

3.1.1. Characterization of powders

The ThO_2–30%UO_2 and ThO_2–50%UO_2 powders obtained by co-precipitation process were characterized by the following techniques:

- O/M ratio by thermogravimetry.
- Crystal structure and phase analysis (XRD).
- Surface area measurement (BET).
- Particle size (XRD, Laser analysis).
- Microstructure (SEM, EPMA).
- Carbon analysis (combustion).

The O/M ratio of the powder was measured thermogravimetrically using Bahr (Model STA-503) thermal analyzer. The accuracy of the measurement in weight was within ±1 μg. The O/M ratio of the powder was obtained from the weight decrease of this sample on heating in Ar–8%H_2 at 800 °C at which the O/M ratio is 2.00. The phase analysis was performed using X-ray diffractometry (Diano make, model XRD-8760). The X-ray diffraction patterns of the pellets were obtained by using Cu Kα radiation monochromatized with curved graphite monochromator. The accuracy of this equipment is ±5%. The high angle scan was carried out from 100 to 145° (2θ) with a step size of 0.5°/min. The lattice parameters were calculated from this high angle scan by least squares method. Further from the XRD data, the crystallite size was estimated. For this, scan was carried at a low speed of 0.02°/min and crystallite size was determined from the line broadening of the XRD peaks. The particle size was also determined using laser based particle size analyzer which employs the time of transit theory. The specific surface area of the powder was measured using the Brunauer–Emmett–Teller (BET) method with helium as the adsorbate gas. The powder samples for surface area analysis were rinsed in distilled water and dried in a vacuum prior to the BET analysis to remove all fine particulates. The particle shape was determined by SEM (Philips make, model XL-30). Differential thermal analysis (DTA) was carried out using Bahr (Model STA-503) thermal analyzer in Ar from room temperature to 1500 °C to study the stability of the powders at high temperatures. The carbon content was determined by combustion. The sample was burnt in a stream of oxygen and the CO_2 evolved was measured quantitatively by thermal conductivity method. The uncertainty of the methods was ±2% for carbon.

Table 1
Chemical analysis for co-precipitated (Th–U)O_2 powders.

Composition	Ratio of Th: U (wt%)
ThO_2–30%UO_2	70.7: 29.3
ThO_2–50%UO_2	50.1: 49.9

Table 2
Impurities in the (Th,U)O_2 powders made by co-precipitation.

Element	ThO_2–50%UO_2 (ppm)	ThO_2–30%UO_2 (ppm)
B	0.1	0.3
Cd	<0.1	<0.1
Co	<5	<5
Ca	<5	<5
Fe	<10	<10
Si	<40	<40
Al	43.4	36.8
Mn	<2	<2
W	<40	<40
Cr	<5	<5
Pb	9.1	12.5
Mo	19.6	30.6
Ni	23.2	20.5
Na	<5	<5
V	<5	<5
Zn	<10	<10

3.2. Fabrication of pellets

The procedure for the fabrication of ThO_2–30%UO_2 and ThO_2–50%UO_2 green pellets consists of the following steps:

(a) Milling of the co-precipitated ThO_2–UO_2 powder in a planetary ball mill for 4 h with tungsten carbide balls.
(b) Double precompaction of the above prepared mixtures at 150 MPa.
(c) Granulation of the precompacts.
(d) Final cold compaction of the granulated powder at 300 MPa into green pellets.

The green density of the compacts was around 62% of the theoretical density. To facilitate compaction and to impart larger handling strength to the green pellets, 1 wt% zinc behenate was added as lubricant/binder at the last 1 h of the mixing/milling procedure. The green pellets were 8.1 mm in diameter and around 7 mm in length. The resulting pellets were sintered at 1400 °C in air for 6 h. The entire flow-sheet of fabrication of ThO_2–UO_2 pellets by co-precipitation process is given in Fig. 1.

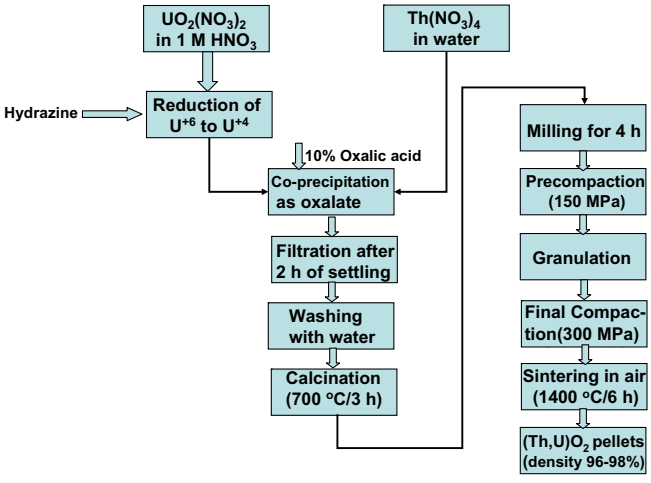

Fig. 1. Flow-sheet of fabrication of ThO_2–UO_2 pellets by co-precipitation process.

3.2.1. Characterization of pellets

The ThO_2–30%UO_2 and ThO_2–50%UO_2 pellets were characterized by their density, O/M ratio, phases, microstructures and homogeneity. For metallographic analysis, the sintered pellet in air was mounted on a support with Araldite cement and ground by the emery papers of successive grades. The final polishing was done using diamond paste. The pellet was then removed from the mount by dissolving the cement by acetone and then etched thermally by holding it at 1500 °C for 4 h in air. The grain size was determined by the intercept method. The microstructure was characterized by SEM. The uranium distribution in the sintered pellet was determined by EPMA (Cameca, model Sx-100).

4. Results

The O/M ratios of the calcined (in air 700 °C for 3 h) ThO_2–30%UO_2 and ThO_2–50%UO_2 powders produced by co-precipitation method were found to be 2.218 and 2.301, respectively. The XRD powder patterns of these samples are shown in Fig. 2. Both ThO_2–30%UO_2 and ThO_2–50%UO_2 are two phase mixtures of CaF_2 type solid solution and U_3O_8. The lattice parameters were calculated from the high angle scans (2θ = 100–145°) using Nelson–Riley extrapolation method. The lattice parameters of ThO_2–30%UO_2 and ThO_2–50%UO_2 powders were found to be 0.55519 nm and 0.55205 nm, respectively. The high angle XRD pattern shown in Fig. 3 indicates the solid solution formation of the co-precipitate powders. Table 3 lists the lattice parameters and phases present in the powders of the above compositions. From the O/M ratios and the lattice parameter data, the amount of U_3O_8 present in the above powders was estimated. The estimation was made from the assumption that for high O/M values, ThO_2 forms a solid solution with $UO_{2.25}$. The remaining UO_2 is assumed to exist as U_3O_8. The amount of U_3O_8 present in ThO_2–30%UO_2 and ThO_2–50%UO_2 powders was calculated and found to be 9.88 and 14.19 mol%, respectively.

Table 3
Lattice parameter, O/M ratio and the amount of U_3O_8 in (Th,U)O_2 powders after heated in air at 700 °C for 3 h.

Material	Lattice parameter, nm	O/M	y in $(Th_{1-y}U_y)O_{2+x}$	Mol% U_3O_8
ThO_2–30%UO_2	0.55519	2.218	0.2818	9.88
ThO_2–50%UO_2	0.55205	2.301	0.4781	14.19

The average particle sizes of the ThO_2–30%UO_2 and ThO_2–50%UO_2 powders were found to be 0.63 ± 0.21 and 0.81 ± 0.17 μm, respectively. The particle distribution and the volume cumulative graphs for ThO_2–30%UO_2 and ThO_2–50%UO_2 powders are shown in Figs. 4 and 5, respectively. From these figures, it may be noted that about 90% particles for ThO_2–30%UO_2 and ThO_2–50%UO_2 are below 1.0 μm. But the size of the ThO_2–

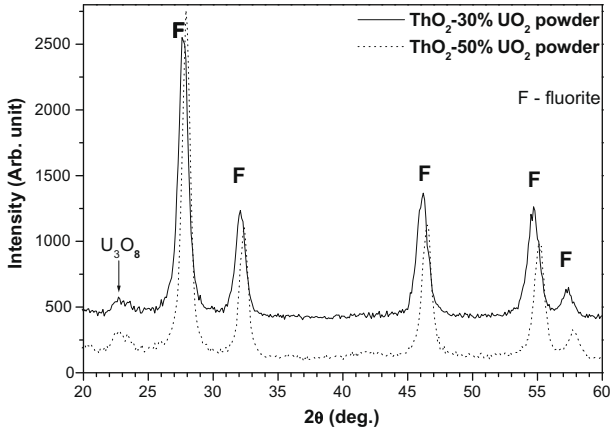

Fig. 2. XRD patterns of ThO_2–30%UO_2 and ThO_2–50%UO_2 powders made by co-precipitation process.

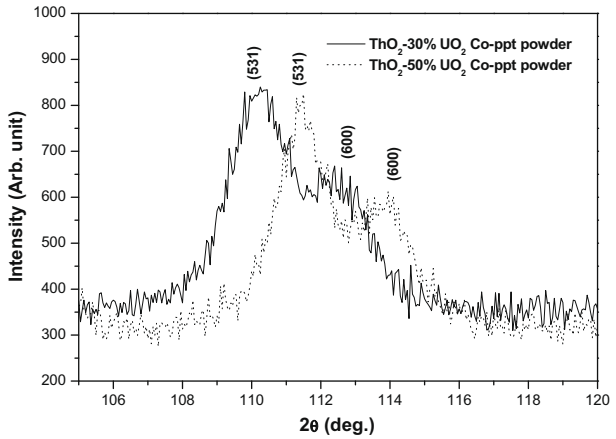

Fig. 3. XRD patterns of ThO_2-30%UO_2 and ThO_2–50%UO_2 powders at higher angles for the determination of lattice parameters.

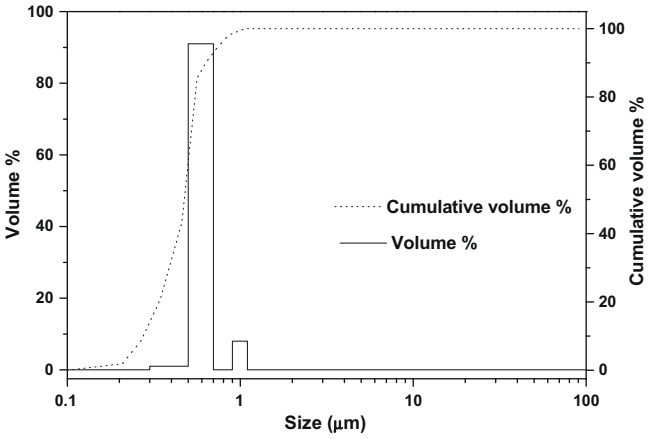

Fig. 4. Particle size and the volume cumulative graphs for ThO_2–30%UO_2 powder.

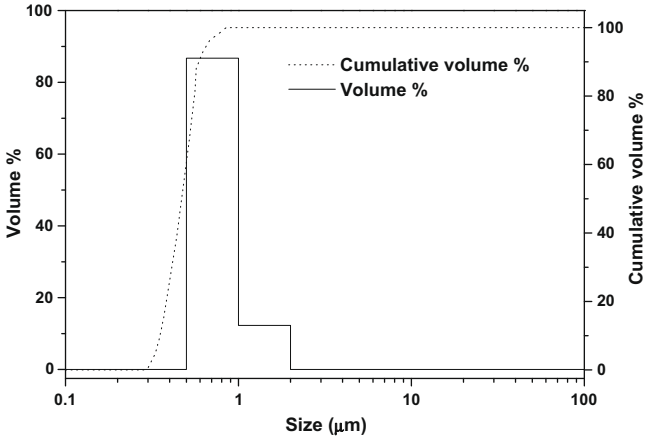

Fig. 5. Particle size distribution of ThO_2–50%UO_2 powder made by co-precipitation process.

50%UO_2 powder was found to be slightly larger than that of the ThO_2–30%UO_2 powder. The figures show that the distribution of particle size is sharp for ThO_2–50%UO_2 powder with most particles in a range between 0.55 and 2.0 μm. The surface area values for ThO_2–30%UO_2 and ThO_2–50%UO_2 powders were 12.10 and 7.16 m^2/g, respectively. A close examination on the shape of the above mentioned powders was carried by SEM. The ThO_2–50%UO_2 particles were more spherical, while the ThO_2–30%UO_2 particles exhibited irregular surfaces with angular appearance. The carbon content of the powders was found to be 2500 ppm.

Fig. 6 shows the XRD patterns of the ThO_2–30%UO_2 and ThO_2–50%UO_2 pellets sintered in air at 1400 °C for 6 h after co-precipitation. The patterns are similar to those of the calcined powders of the same composition (Fig. 2, 700 °C, in air). The XRD results for sintered ThO_2–30%UO_2 and ThO_2–50%UO_2 pellets showed that the U_3O_8 phase still exists together with the fluorite phase. The O/M ratios for the above composition were 2.170 and 2.230, respectively. But the amount of U_3O_8 present in both the pellets was less than that present in the corresponding powders. For ThO_2–30%UO_2 composition, the amount of U_3O_8 present in the powder has come down on sintering in air at 1400°C for 6 h from 9.88 to 6.05 mol%. Similarly, for ThO_2–50%UO_2 composition, it has come down from 14.19% to 7.50%. These results clearly indicate that the U_3O_8 amount decreases with dissolution into UO_{2+x} during heating the sample forming solid solution with ThO_2. Table 4 gives details of the lattice parameters and phases present for the above compositions. The lattice parameters of the samples of both compositions decreased on sintering in air. This again indicates that more UO_2 has gone to ThO_2 lattice on sintering at 1400 °C for 6 h.

As-polished microstructure of co-precipitated pellets showed very fine pore structure. Most of the pores were in the range of 2–3 μm. Occasionally a few patches of dense areas are seen. A few lenticular pores were also noticed especially in ThO_2–30%UO_2 pellet. Typical as-polished microstructures for ThO_2–30%UO_2 and ThO_2–50%UO_2 pellets are shown in Fig. 7. The ThO_2–30%UO_2 pellet after thermal etching is rather uniform. For ThO_2–50%UO_2 pellet, one or two patches consisting of bigger grains (40 μm) were seen (Fig. 8). The grain sizes determined by intercept method were found to be 5.7 and 4.5 μm for ThO_2–30%UO_2 and ThO_2–50%UO_2, respectively. The SEM photograph of ThO_2–30%UO_2 pellet sintered in air is shown in Fig. 9. In order to know the distribution of Th, U and O, electron beam scanning was performed by EPMA across the pellet from centre to periphery. A typical result of X-ray intensities of

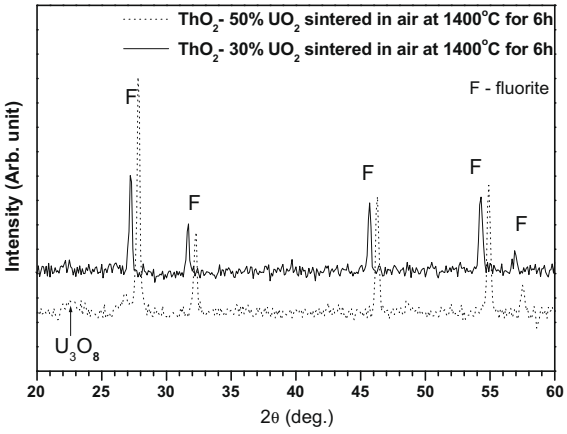

Fig. 6. XRD patterns of ThO_2–30%UO_2 and ThO_2–50%UO_2 pellets sintered in air made by co-precipitation process.

Table 4
Lattice parameter, O/M ratio and the amount of U_3O_8 in $(Th,U)O_2$ pellets after sintered in air at 1400 °C for 6 h.

Material	Lattice parameter, nm	O/M	y in $(Th_{1-y}U_y)O_{2+x}$	$2+x$ in $(Th_{1-y}U_y)O_{2+x}$	Mol% U_3O_8
ThO_2–30%UO_2	0.55497	2.170	0.2956	2.074	6.05
ThO_2–50%UO_2	0.55178	2.230	0.4950	2.123	7.50

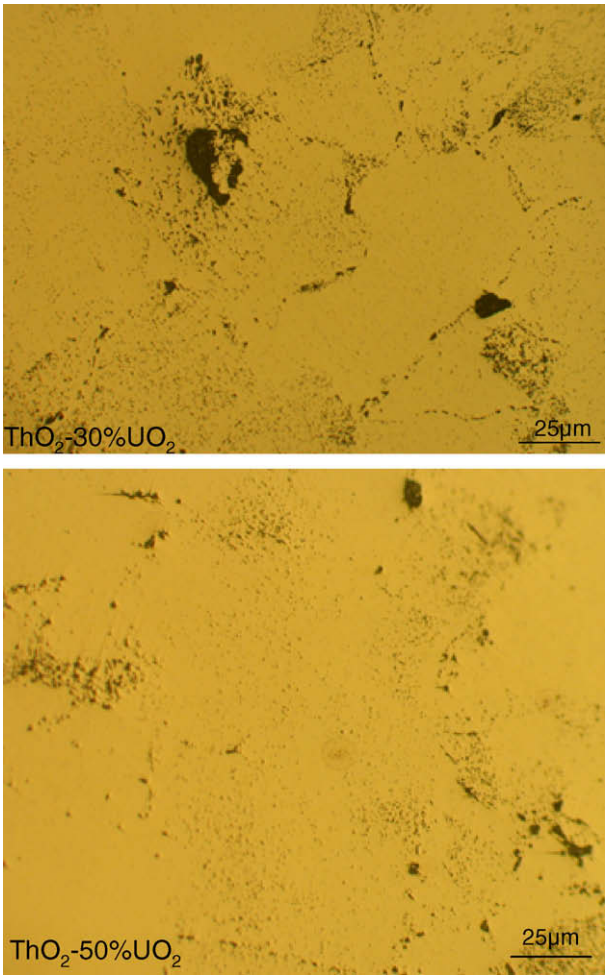

Fig. 7. Typical as-polished microstructures for ThO_2–30%UO_2 and ThO_2–50%UO_2 pellets.

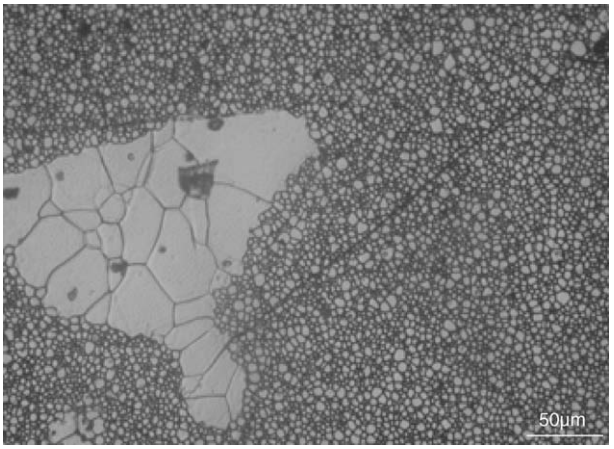

Fig. 8. Microstructure of a ThO_2–50%UO_2 pellet sintered in air showing patches of bigger grains.

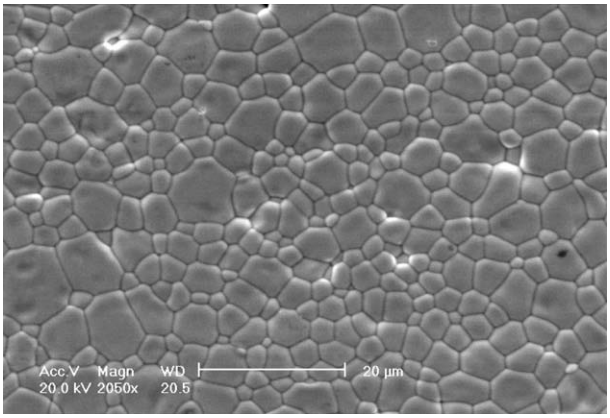

Fig. 9. Microstructure of ThO_2–30%UO_2 pellet. Pellet: sintered in air and etched thermally.

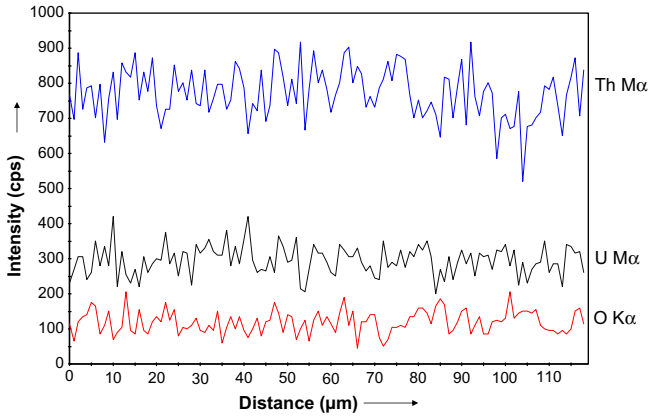

Fig. 10. X-ray line scan for Th M_α, U M_α and O K_α across the grain structure for ThO_2–30%UO_2.

Th M_α, U M_α and O K_α is shown in Fig. 10. It shows the essentially uniform U distribution in the pellet. The significant results are summarized below:

1. ThO_2–30%UO_2 and ThO_2–50%UO_2 powders prepared by co-precipitation method showed O/M ratios of 2.218 and 2.301, respectively.
2. The XRD results for ThO_2–30%UO_2 and ThO_2–50%UO_2 powders showed that they were two phase mixtures of fluorite-type solid solution and U_3O_8.
3. The average particle sizes of the ThO_2–30%UO_2 and ThO_2–50%UO_2 powders were found to be 0.63 ± 0.21 and 0.81 ± 0.17 µm, respectively.
4. The XRD data for sintered ThO_2–30%UO_2 and ThO_2–50%UO_2 showed that the amount of U_3O_8 present in the pellet (1400 °C, in air) samples was less than that in the powders (700 °C, in air).
5. The grain sizes determined by intercept method were 5.7 and 4.5 µm for ThO_2–30%UO_2 and ThO_2–50%UO_2, respectively.
6. The EPMA data confirmed that the distribution of uranium in the pellet was essentially uniform for both the oxides.

5. Discussion

From the results given in Section 4. Results, it is clear that good quality ThO_2–UO_2 powders can be made using the co-precipitation process from uranyl nitrate and thorium nitrate solutions. As mentioned in Chapter 4, the XRD patterns for ThO_2–30%UO_2 and ThO_2–50%UO_2 powders heated in air at 700 °C were of two phase mixtures consisting of fluorite-type solid solution and U_3O_8. Considering the heating conditions of 700°C in air, the co-existence of U_3O_8 is not surprising. The reduction treatment by H_2 was intentionally not performed in the present study because it has been shown that the presence of U_3O_8 helps to enhance sintering [32]. The above results also imply that the ThO_2–30%UO_2 and ThO_2–50%UO_2 pellets could be fabricated using the powders obtained by the co-precipitation technique which yielded densities in the range of 96–98% T.D. when they were sintered in air at 1400 °C. Since sintering is done in air, it is economically beneficial without the use of costly cover gases such as Ar or Ar–H_2 [33,34]. Also, costly furnaces and sintering boats made of Mo or W indispensable to heating in reducing atmospheres are not needed.

Solid UO_2 and ThO_2 form a continuous series of solid solutions [35–37]. Lattice parameter measurements of ThO_2–UO_2 solutions show that, within experimental accuracy, Vegard's law is obeyed. Anderson et al. [38] observed that the lower limit of the stable temperature range of the ThO_2–UO_2 solid solution phase in air lowers to 1400 °C if the concentration of UO_2 is lower than 78 mol%. In the solid solution phase of UO_2 concentrations 15–78 mol%, the excess oxygen atoms are deduced to occupy the interstitial sites in the fluorite lattice. It has been reported that the solid state solubility of U_3O_8 in ThO_2 is negligibly small [32,39,40]. Hund and Niessen [41] studied the phase relations in the ThO_2–U_3O_8–O_2 system. According to them, U_3O_8 phase was precipitated in the solid solution phase at higher U_3O_8 concentrations, but a single phase region of the cubic solid solution was observed to exist at lower U_3O_8 concentrations. Kutty et al. [42,43] have demonstrated that the addition of small quantities of U_3O_8 to ThO_2 enhances sintering, resulting in formation of high quality ThO_2–UO_2 pellets without the use of conventional dopants such as CaO and Nb_2O_5, which also causes to reduce the impurity level in the pellets. The significance of U_3O_8 addition for enhancing sintering, especially in UO_2, has been discussed by many researchers [42–44]. Chevrel et al. [44] indicated that the composition of $UO_{2.25}$ appeared to be the most appropriate for the low temperature sintering. This overall composition is obtained by the addition of U_3O_8 powder to UO_2. With the above background in mind, we will analyze the fabrication of ThO_2–UO_2 powders made by co-precipitation process and its sintering behaviour in oxidizing atmosphere.

5.1. Powder

The powders produced by co-precipitation process had larger surface area and smaller particle size than those made by the conventional solid state mixing route. The surface area of ThO_2 and UO_2 powder made by the latter method generally lies in a range 2–3 m^2/g. But the surface areas of co-precipitated ThO_2–30%UO_2 and ThO_2–50%UO_2 powders were found to lie between 12.10 and 7.16 m^2/g. The O/M ratios of the above powders were also higher as were 2.218 and 2.301, respectively. To study the stability of the above powders at high temperatures, thermogravimetric analysis of ThO_2–30%UO_2 and ThO_2–50%UO_2 powders has been carried out up to 1500°C and the resultant thermograms are given in Fig. 11. Here the weight change is plotted against temperature when the powder of ThO_2–UO_2 sample was heated in Ar at a heating rate of 10 K/min. The weight loss was slow up to 700 °C but it became more prominent above that temperature. It is evident that even at 1500 °C the loss in weight has not been completed. The total weight loss for ThO_2–50%UO_2 powder was around 3%. For ThO_2–30%UO_2 powder the weight loss was less than that for ThO_2–50%UO_2. The powders after the thermogravimetric test were collected and O/M ratio of the above powders was redetermined.

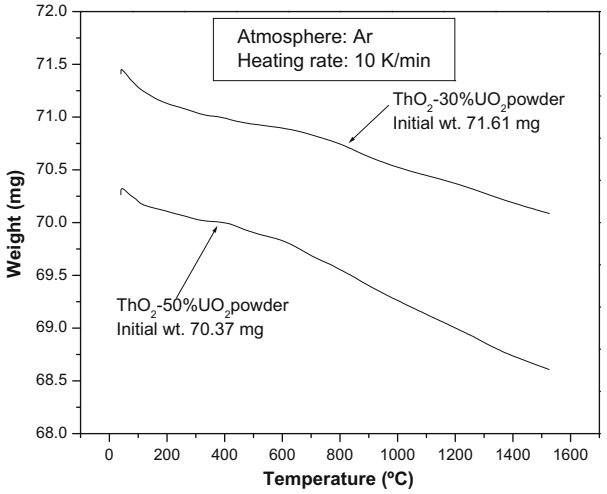

Fig. 11. Thermogravimetric curve showing weight change of ThO_2–30%UO_2 and ThO_2–50%UO_2 powders when heated in argon.

The O/M ratios of ThO_2–30%UO_2 and ThO_2–50%UO_2 powders after heating in Ar up to 1500 °C were found to be 2.07 and 2.11, respectively. This study clearly shows that the co-precipitated powders were still losing oxygen continuously on heating up to1500 °C. The results are similar to our earlier study [43], where the mixture of ThO_2 and U_3O_8 was heated in Ar up to 1400 °C. The conclusion was that the loss in weight was not completed even at this temperature showing that a decreased amount of U_3O_8 still existed together with ThO_2–UO_{2+x} at this temperature. The XRD data of the present study suggest that the phases present in the co-precipitated powders are ThO_2–$UO_{2.25}$ and U_3O_8. But on heating, U_3O_8 decomposed to UO_{2+x} and reaches the composition of $UO_{2.25}$. This newly formed $UO_{2.25}$ is considered to dissolve in ThO_2–$UO_{2.25}$ forming solid solution. It has been reported that ThO_2 added to UO_2 in a small amount acts as inert diluents but if the amount is large it affects to stabilize the fluorite structure by suppressing oxidation of uranium cations [29]. Actually, the measured oxygen potential of $(Th,U)O_{2+x}$ solid solution is significantly higher than that of UO_{2+x} [39,45]. These experimental facts support the increased resistibility of $(Th,U)O_{2+x}$ against oxidation.

5.2. Sintering

The diffusion of metal atoms depends on the concentration of structural imperfections such as metal vacancies. This concentration changes with temperature, atmosphere and dopants [46–50]. The sintering temperature can be lowered either by heating in an appropriate atmosphere or by the addition of dopant. For uranium dioxide, the oxidizing atmosphere has been used for lowering the sintering temperature from 1700 to 1300 °C. In the case of thorium dioxide, dopants have been effectively used for lowering the sintering temperature from 1700 to 1250 °C.

The findings given in Section 4. Results show that the starting $(Th,U)O_2$ powder made by co-precipitation route has a higher O/M ratio and larger surface area and has two phases. Such properties of surface area and O/M ratio help to have higher density pellets after sintering. When the green compacts were sintered in air at 1400 °C for 6 h, the final densities obtained were in the range of 96–98% T.D. The high densities obtained in this study are due to the following factors:

1. High surface area of the starting powders.
2. Higher O/M ratio of the powders.
3. Presence of a small amount of U_3O_8 phase.

The larger surface area corresponds to higher surface energy. The driving force for sintering is the reduction in surface energy. The higher O/M ratio indicates the presence of higher concentration of oxygen interstitials. Lay and Carter [51] have shown that the self-diffusion coefficient of uranium in UO_{2+x} is proportional to x^2. This is predominantly due to the increased concentration of uranium vacancies in UO_{2+x}. It has been established that U_3O_8 acts as a sintering aid for ThO_2 [42,43]. The O/U values of U_3O_{8-z} oxide in air at 1000, 1100 and 1200°C are calculated 2.637, 2.633 and 2.627, respectively [43]. This means that on increasing the temperature, there may be a considerable amount of deviation from stoichiometry generating more point defects. Therefore, the presence about 10–14 mol% U_3O_8 in the ThO_2–30%UO_2 and ThO_2–50%UO_2 powders helped in achieving higher density.

The O/M ratios of the sintered ThO_2–30%UO_2 and ThO_2–50%UO_2 pellets were 2.170 and 2.230, respectively (Table 4), which are lower than those of the corresponding powders before sintering. Using the lattice parameter of the cubic fluorite-type solid solution and the bulk O/M ratio, the uranium concentration in the solid solution was calculated. Table 4 shows that about 3–7 mol% U_3O_8 was decomposed and additionally dissolved in $(Th,U)O_2$ during the sintering. In the mixture of ThO_2–UO_{2+x} and U_3O_8, the densification at high temperatures probably proceeds as follows [52–54]:

1. Formation of defective structured U_3O_{8-z}.
2. Dissolution of a part of U_3O_{8-z} to UO_{2+x}.
3. Solid solution formation between $(Th,U)O_2$ and UO_{2+x}.
4. Simultaneous sintering of $(Th,U)O_2$.

6. Conclusions

The co-precipitation method was found to be suited for obtaining mixed oxide pellets of high density and excellent microhomogeneity. ThO_2–30%UO_2 and ThO_2–50%UO_2 pellets were fabricated using the powders obtained by the co-precipitation method, and these pellets were characterized by means of optical microscopy, XRD, SEM and thermogravimetry. The conclusions are as follows:

1. ThO_2–30%UO_2 and ThO_2–50%UO_2 powders prepared through the co-precipitation route showed higher O/M ratios of 2.218 and 2.301, respectively. On sintering in air at 1400 °C, the O/M ratio of the above decreased to 2.170 and 2.230, respectively.
2. The XRD analysis revealed that ThO_2–30%UO_2 and ThO_2–50%UO_2 powders heated in air at 700 °C were two phase mixtures composed of cubic fluorite solid solution and U_3O_8 phases.
3. The amount of U_3O_8 phase present in ThO_2–30%UO_2 and ThO_2–50%UO_2 powders decreases after sintering the pellet in air 1400 °C, which suggests that a part of U_3O_8 was decomposed and dissolved in the $(Th,U)O_{2+x}$ phase during sintering forming solid solution.
4. The average grain sizes of sintered ThO_2-30%UO_2 and ThO_2–50%UO_2 pellets were 5.7 and 4.5 μm, respectively. ThO_2–50%UO_2 pellet showed one or two patches consisting of bigger grains of about 40 μm.

References

[1] K.C. Radford, R.J. Bratton, J. Nucl. Mater. 57 (1975) 287.
[2] M. Freshley, Nucl. Technol. 15 (1972) 239.
[3] M.D. Freshley, D.W. Brite, J.L. Daniel, P.E. Hart, J. Nucl. Mater. 81 (1979) 63.
[4] J. Vandezande, in: Advanced Methods of Process/Quality Control in Nuclear Reactor Fuel Manufacture, IAEA-TECDOC-1166, International Atomic Energy Agency, Vienna, 1999, p. 59.
[5] P.K. Ivison, P.M.A. Cook, S. Bremier, C.T. Walker, Nuclear Fuel Behaviour Modelling at High Burnup and its Experimental Support, IAEA-TECDOC-1233, International Atomic Energy Agency, Vienna, 2001, p. 239.

[6] H.J. Matzke, in: T. SØrensen (Ed.), Non-Stoichiometric Oxides, Academic Press, New York, 1981, p. 156.
[7] D.R. Olander, Fundamental Aspects of Nuclear Reactor Fuel Elements, TID-26711-P1 (US Department of Energy, 1976) p. 145.
[8] J.R. Kennedy et al., Advances for Future Nuclear Fuel Cycles, Atalante, France, June 21–24, 2004.
[9] B.H. Lee, Y.H. Koo, D.S. Sohn, Nuclear Fuel Behaviour Modelling at High Burnup and its Experimental Support, IAEA-TECDOC-1233, International Atomic Energy Agency, Vienna, 2001, p. 247.
[10] A.G. Leyva, D. Vega, V. Trimacor, D. Mar, J. Nucl. Mater. 303 (2002) 29.
[11] Status and Advances in MOX Fuel Technology, Technical Report Series No. 415, International Atomic Energy Agency, Vienna, 2003, p. 16.
[12] H.J. Matzke, J. Chem. Soc. Faraday Trans. 86 (1990) 1243.
[13] H. Bairiot, MOX Fuel Cycle Technologies for Medium and Long Term Deployment, C&S Papers Series No. 3/P, International Atomic Energy Agency, Vienna, 2000, p. 81.
[14] D. Hugelmann, D. Greneche, MOX Fuel Cycle Technologies for Medium and Long Term Deployment (Proc. Symp. Vienna, 1999), C&S Papers Series No. 3/P, IAEA, Vienna (2000), pp. 102–108.
[15] P.D. Wilson (Ed.), The Nuclear Fuel Cycle – From Ore to Waste, Oxford University Press, Oxford, 1996.
[16] B.S. Zakharkin, MOX Fuel Cycle Technologies for Medium and Long Term Deployment (Proc. Symp. Vienna, 1999), C&S Papers Series No. 3/P, IAEA, Vienna, 2000, p. 146.
[17] L. Kincaid, E. Aitken, I. Taylor, Trans. Am. Nucl. Soc. 33 (1979) 470.
[18] V. Sneider, F. Hermann, W. Druckenbrodt, Trans. Am. Nucl. Soc. 31 (1979) 176.
[19] R.B. Grover, S. Chandra, A Strategy for Growth of Electrical Energy in India, Government of India, Department of Atomic Energy, August 2004.
[20] R.K. Sinha, A. Kakodkar, Nucl. Eng. Des. 236 (2006) 683.
[21] R. Chidambharam, Atom. Peace Int. J. 1 (2006) 137.
[22] Thorium Fuel Cycle – Potentials Benefits and Challenges, IAEA-TECDOC-1450, International Atomic Energy Agency, Vienna, 2005, p. 1.
[23] Y. Atlas, M. Eral, H. Tel, J. Nucl. Mater. 249 (1997) 46.
[24] G. Rousseau, M. Fattahi, F. Boucher, G. Ouvrard, Radiochim. Acta 90 (2003) 523.
[25] H.J. Matzke, J. Van Geel, J. Magill, Top Fuel '97, vol. I, BNES, London, 1997. p. 4.32.
[26] International Atomic Energy Agency, Thorium Fuel Utilization: Options and Trends, IAEA-TECDOC-1319, Vienna, 2002.
[27] I.S. Kurina, L.S. Gudkov, V.N. Rumyantsev, Atom. Energy 92 (2002) 461.
[28] G.D. White, L.A. Bray, P.E. Hart, J. Nucl. Mater. 961 (1981) 305.
[29] L. Argo, Experimental Determination of the Dry Oxidation Behavior of a Compositional Range of Uranium–Thorium Mixed-Oxide Pellet Fragments, MS Thesis, University of Florida, 2003.
[30] P.S. Dhami, R. Kannan, K.S. Rao, R. Shyam Lal, K. Kumarguru, Ajithlal, Nitin Sinalkar, A. Dakshinamoorthy, U. Jambunathan, P.K. Dey, NUCAR, 2005, p. 215.
[31] K.Sreenivasa Rao, R. Shyam Lal, C.V. Narayanan, U. Jambunathan, A. Ramanujam, V.P. Kansra, BARC Report No. BARC/2003/E009, 2003.
[32] T.R.G. Kutty, K.B. Khan, P.S. Somayajulu, A.K. Sengupta, J.P. Panakkal, Arun Kumar, H.S. Kamath, J. Nucl. Mater. 373 (2008) 299.
[33] C.R.A. Catlow, A.B. Lidiard, Proceedings of the Symposium Themodynamics of Reactor Materials, vol. II, IAEA, Vienna, 1974, p. 27.
[34] H.J. Matzke, Philos. Mag. A 64 (1991) 1181.
[35] J.A. Christensen, General Electric Report HW-76559, 1962, p 11.
[36] R.E. Latta, E.C. Duderstadt, R.E. Fryxell, J. Nucl. Mater. 35 (1970) 347.
[37] I. Cohen, R.M. Berman, J. Nucl. Mater. 18 (1966) 77.
[38] J.S. Anderson, D.N. Edgington, L.E.J. Roberts, E. Wait, J. Chem. Soc. 76 (1954) 3324.
[39] K. Bakker, E.H.P. Cordfunke, R.J.M. Konings, R.P.C. Schram, J. Nucl. Mater. 250 (1997) 1.
[40] R. Paul, C. Keller, J. Nucl. Mater. 41 (1971) 133.
[41] F. Hund, G. Niessen, Z. Elekrochem. 56 (1952) 972.
[42] T.R.G. Kutty, K.B. Khan, P.V. Hegde, A.K. Sengupta, S. Majumdar, H.S. Kamath, Sci. Sintering 35 (2003) 125.
[43] T.R.G. Kutty, P.V. Hegde, K.B. Khan, T. Jarvis, A.K. Sengupta, S. Majumdar, H.S. Kamath, J. Nucl. Mater. 335 (2004) 462.
[44] H. Chevrel, P. Dehaudt, B. Francois, J.F. Baumard, J. Nucl. Mater. 189 (1992) 175.
[45] R.P.C. Schram, J. Nucl. Mater. 344 (2005) 223.
[46] F. Thummler, W. Thomma, Metall. Rev. 115 (1967) 69.
[47] D.L. Johnson, T.M. Clarke, Acta Met. 12 (1964) 1173.
[48] R.L. Coble, J. Am. Ceram. Soc. 41 (1958) 55.
[49] W.D. Kingery, M. Berg, J. Appl. Phys. 26 (1955) 1205.
[50] R.W. Cahn, P. Haasen, E.J. Krammer, B.R.T. Frost, Materials Science and Technology, A Comprehensive Review, vol. 10A, VCH Publishers, New York, 1994. p. 114.
[51] K.W. Lay, R.E. Carter, J. Nucl. Mater. 30 (1969) 74.
[52] H. Assmann, W. Doerr, M. Peehs, J. Nucl. Mater. 140 (1986) 1.
[53] Kun Woo Song, Keon Sik Kim, Ki Won Kang, Youn Ho Jung, J. Nucl. Mater. 317 (2003) 204.
[54] P. Balakrishna, B.P. Varma, T.S. Krishnan, T.R.R. Mohan, P. Ramakrishnan, J. Nucl. Mater. 160 (1988) 88.